Electrostatic Potential at the Retinal of Three Archaeal Rhodopsins: Implications for Their Different Absorption Spectra

Edda Kloppmann, Torsten Becker, and G. Matthias Ullmann*
Structural Biology/Bioinformatics, University of Bayreuth, Bayreuth, Germany

ABSTRACT **The color tuning mechanism of the rhodopsin protein family has been in the focus of research for decades. However, the structural basis of the tuning mechanism in general and of the absorption shift between rhodopsins in particular remains under discussion. It is clear that a major determinant for spectral shifts between different rhodopsins are electrostatic interactions between the chromophore retinal and the protein. Based on the Poisson-Boltzmann equation, we computed and compared the electrostatic potential at the retinal of three archaeal rhodopsins: bacteriorhodopsin (BR), halorhodopsin (HR), and sensory rhodopsin II (SRII) for which high-resolution structures are available. These proteins are an excellent test case for understanding the spectral tuning of retinal. The absorption maxima of BR and HR are very similar, whereas the spectrum of SRII is considerably blue shifted—despite the structural similarity between these three proteins. In agreement with their absorption maxima, we find that the electrostatic potential is similar in BR and HR, whereas significant differences are seen for SRII. The decomposition of the electrostatic potential into contributions of individual residues, allowed us to identify seven residues that are responsible for the differences in electrostatic potential between the proteins. Three of these residues are located in the retinal binding pocket and have in fact been shown to account for part of the absorption shift between BR and SRII by mutational studies. One residue is located close to the β-ionone ring of retinal and the remaining three residues are more than 8 Å away from the retinal. These residues have not been discussed before, because they are, partly because of their location, no obvious candidates for the spectral shift among BR, HR, and SRII. However, their contribution to the differences in electrostatic potential is evident. The counterion of the Schiff base, which is frequently discussed to be involved in the spectral tuning, does not contribute to the dissimilarities between the electrostatic potentials. Proteins 2005; 61:953–965.** © 2005 Wiley-Liss, Inc.

Key words: bacteriorhodopsin; halorhodopsin; sensory rhodopsin II; spectral tuning; opsin shift; continuum electrostatics; electrostatic potential; Poisson-Boltzmann equation

INTRODUCTION

Light is one of the most important factors for life. The conversion of light into chemical energy during photosynthesis constitutes the main source of energy for living organisms. However, light is not only used as an energy source but also as an external signal. In phototaxis, for instance, single-cell organisms use light signals to escape harmful and search for favorable light conditions. In higher organisms, light receptors in complex signaling systems provide the means for vision. Chromophore-binding proteins can tune the absorption of these chromophores by specific interactions to an exact maximum.

Color tuning of rhodopsins has been in the focus of research for decades.[1,2] This protein family is of particular interest, in part because the visual pigments belong to this class and the comprehension of the tuning mechanism will further the understanding of color vision and, in part, because of the extreme variation of absorption maxima in this protein family—ranging from ultraviolet to the far red.[3,4] However, despite considerable theoretical[5–15] and experimental[16–22] effort, the molecular details of the tuning mechanism are still debated.

Rhodopsins are 7-helix-transmembrane proteins that bind their chromophore retinal via a Schiff base linkage to a lysinyl residue as shown in Figure 1(a).[23] A protonated retinal Schiff base absorbs at 440 nm in polar solutions.[24] The absorption shift between a protonated retinal Schiff base in solution and in the protein is termed opsin shift,[16] derived from the term for the apoprotein: opsin.

The following study does, however, not focus on the opsin shift itself, but on the absorption shift between different rhodopsins. We call this shift *inter-protein shift*.

Abbreviations: BR, bacteriorhodopsin; HR, halorhodopsin; SRII, sensory rhodopsin II; LPBE, linearized Poisson-Boltzmann equation; QM, quantum mechanical; MM, molecular mechanical

Grant sponsor: retinal protein Forschergruppe 490 of the Deutsche Forschungsgemeinschaft; Grant number: UL 174/4-1,2.

*Correspondence to: G. Matthias Ullmann, Structural Biology/Bioinformatics, University of Bayreuth, Universitätsstr. 30, BGI, 95447 Bayreuth, Germany. E-mail: Matthias.Ullmann@uni-bayreuth.de

Received 25 May 2005; Revised 11 July 2005; Accepted 20 July 2005

Published online 24 October 2005 in Wiley InterScience (www.interscience.wiley.com). DOI: 10.1002/prot.20744

© 2005 WILEY-LISS, INC.

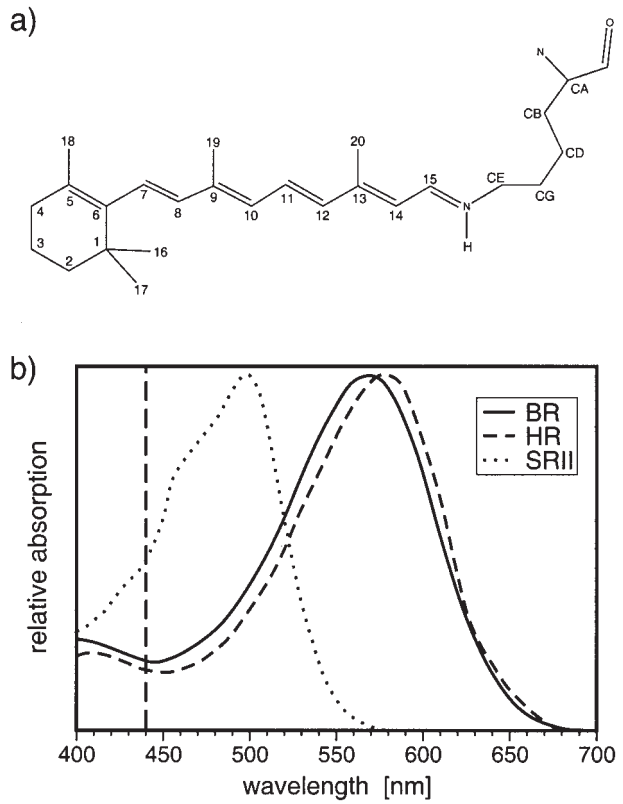

Fig. 1. (**a**) Archaeal rhodopsins bind all-*trans* retinal via a protonated Schiff base linkage to a lysinyl residue. The proton on the Schiff base nitrogen atom is depicted. The β-ionone ring is in 6-s-*trans* conformation. (**b**) Experimental absorption spectra of BR,[40] HR,[41] and SRII.[42] The dotted vertical line indicates the absorption maximum of the protonated retinal Schiff base in methanol solution at 440 nm.

Whereas the opsin shift is a measure for the influence of the protein on the retinal absorption, the inter-protein shift is a measure for the differences in influence the various rhodopsins exert on the absorption of retinal.

Four different rhodopsins are described for halophilic archaea: the proton pump bacteriorhodopsin (BR), the chloride pump halorhodopsin (HR), and two signaling proteins, sensory rhodopsin I and sensory rhodopsin II (SRII).[25–31] In their ground state, these four rhodopsins bind a protonated retinal Schiff base in all-*trans* conformation. High-resolution structures of the ground state are available for BR,[32–36] HR,[37] and SRII.[38,39] These structures are very similar, particularly with regard to the conformation of retinal and the near retinal environment [cf. Fig. 2(a and b)]. Despite the structural similarity, the spectral properties of the proteins differ significantly. Whereas the absorption maxima of BR and HR are at about 570 nm, the absorption maximum of SRII is significantly blue-shifted to about 500 nm [see Fig. 1(b)].[40–42] The absorption spectra of BR, HR, and SRII are shown in Figure 1b. Models describing the inter-protein shift have to account both for the differences between these proteins as well as their similarities. Thus, these archaeal rhodopsins provide an ideal test case for theoretical studies on chromophore tuning.

For the accurate calculation of excitation energies, high-level quantum chemical methods are required. However, present-day limitations of computer resources allow only small molecules to be treated with these methods. The environment of the quantum-chemically treated part may be included using a molecular mechanics force field. The investigation of the influence of this environment is, however, limited by the accuracy of the force field representation and the interaction between the quantum-chemically and the classically treated region. Moreover, molecular dynamics simulations often suffer from convergence problems because of the restricted simulation time. Studies using quantum mechanics/molecular mechanics (QM/MM) methods were able to account for major parts of the observed inter-protein shift between BR and SRII.[9,10] These studies each identified a single residue of the counterion complex to cause the major part of the inter-protein shift. However, they disagree on the nature of this residue.[9,10] Furthermore, mutational studies showed that residues close to the retinal that do not belong to the counterion contribute about 35% to the inter-protein shift between BR and HR.[21] This experimental finding was not reproduced by QM/MM studies so far.[9,10] The structural elements responsible for the inter-protein shift thus remain highly debated and do vary depending on the precise setup of these calculations. Apart from technical details such as the size of the quantum region and its linkage to the classical region, the treatment of environmental effects is crucial for exact calculations.[7,43–46] QM/MM methods have been developed that include polarization of the protein environment and solvent effects.[7,45] Nevertheless, the treatment of the environment remains challenging.

Two major contributions to the inter-protein shift have been discussed in the literature.[6,18,19] The proteins can differ either in their steric or in their electrostatic interaction with the chromophore. Steric interactions may alter the geometry of the chromophore, whereas electrostatic interactions influence its charge distribution. Several facts point toward a minor role of steric interactions for the inter-protein shift of archaeal rhodopsins: (i) It is known that retinal adopts a 6-s-*trans* conformation in all archaeal rhodopsins, in contrast to the 6-s-*cis* conformation favored in solution.[47–49] Thus, the red shift of the absorption spectra upon the 6-s-*cis* to 6-s-*trans* isomerization, which is important for the opsin shift, does not contribute to the inter-protein shift. (ii) The residues close to the retinal are mostly conserved among the archaeal rhodopsins, particularly the aromatic residues which define the shape of the binding pocket. Accordingly, the crystal structures revealed a similar chromophore geometry for BR, HR, and SRII [cf. Fig. 2(a and b)]. In addition, the contribution of induced dipoles to the inter-protein shift that predominantly originate from the π-electrons of aromatic residues is small,[10] because these aromatic residues are conserved among archaeal rhodopsins. This contribution is of importance for the opsin shift as shown by previous calculations.[7,11] (iii) Fourier transform infrared spectroscopy[50] as well as theoretical calculations[10] show that the chromophore geometry is nearly identical in BR and SRII.

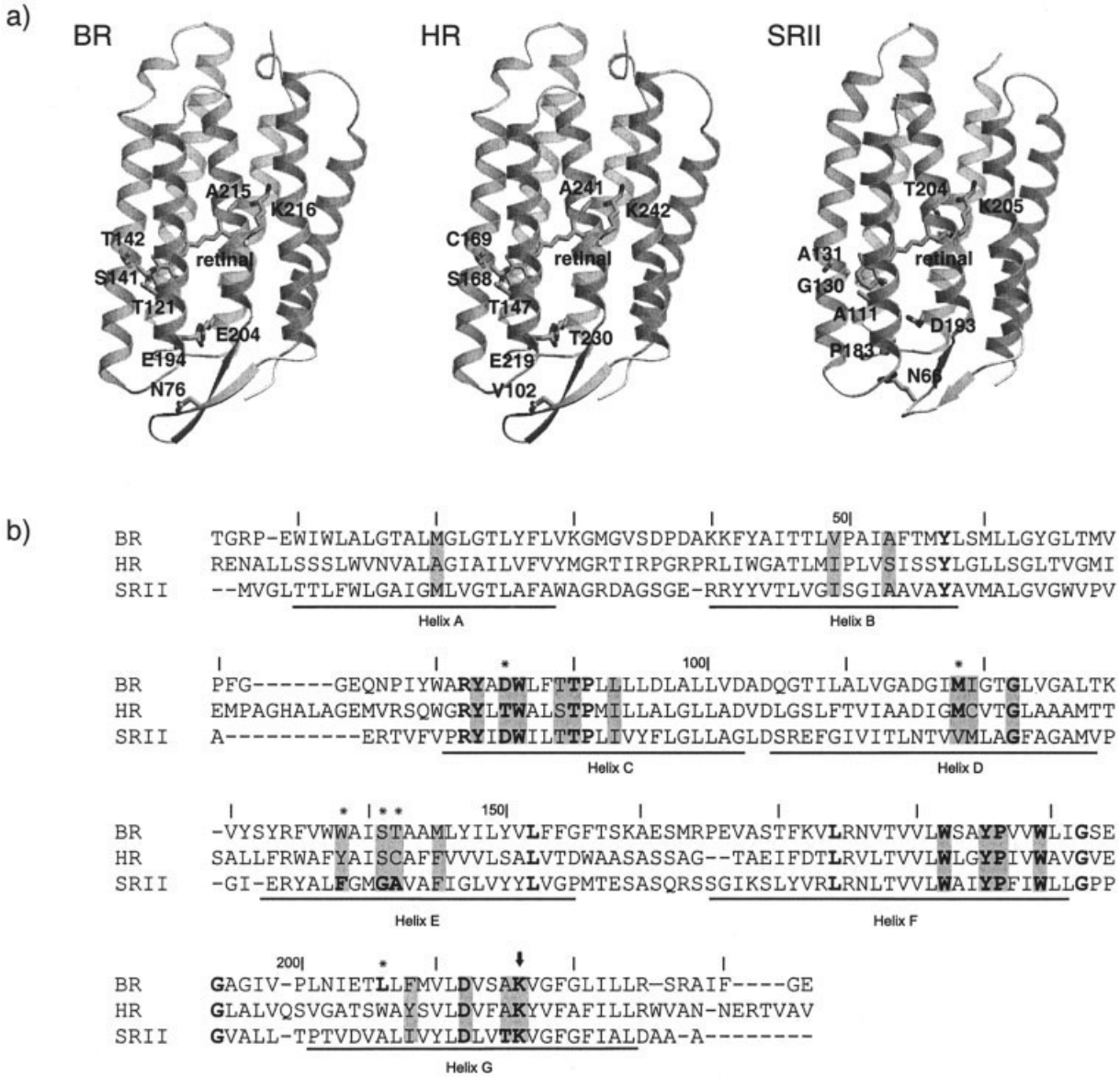

Fig. 2. (**a**) High-resolution X-ray structures of BR, HR, and SRII. The retinal, the lysinyl residue that binds the retinal covalently, and the residues that contribute to the different potential along the retinal π-system are labeled. (**b**) Sequence alignment obtained from the structural alignment of BR, HR, and SRII. The numbering of the residues corresponds to BR. The 24 residues that form the retinal binding pocket are highlighted by gray boxes. The lysinyl residue that binds the retinal covalently to the protein is indicated by a black arrow. Residues that are conserved in BR, HR, or SRII, respectively, are bold and marked by a star. Residues that are conserved throughout the archaeal rhodopsins are bold. The information regarding the conservation is taken from Ref. [29]. The seven transmembrane helixes are indicated by black bars.

Therefore, it seems likely that the major contribution to the inter-protein shift can be attributed to a changed distribution of charges and permanent dipoles.[9,10,50] This electrostatic contribution to the inter-protein shift may be separated into contributions due to the counterion complex and due to other protein residues.

A valid representation of the electrostatics of membrane proteins can be achieved by continuum electrostatic approaches solving the linearized Poisson-Boltzmann equation (LPBE).[51,52] The present work aims to achieve a better understanding of the electrostatic environment of retinal by calculating the potentials created by the protein-membrane system at the retinal.

In this article, we investigate the structural origin of the differences in electrostatic potential among three archaeal rhodopsins: BR, HR, and SRII. The electrostatic potential of the proteins is calculated and compared along the retinal π-system. The differences in electrostatic potential between the proteins can then be related to differences in their absorption behavior. We decomposed the electrostatic potential into contribution of individual residues which allowed us to identify all residues that differ in their

electrostatic potential among BR, HR, and SRII. Mutation studies on binding pocket residues identified several residues that are involved in the inter-protein shift.[21,53] Our calculations are in good agreement with these experimental data. HR, which absorbs at a similar maximum as BR, was included in our calculation. Thus, all results could be tested for similarities between BR and HR and differences between BR and SRII. A model of a particle in a box with a step potential allows us to relate the observed electrostatic potential to the inter-protein shift between the archaeal rhodopsins.

METHODS

Structures

The calculations were performed on high-resolution X-ray structures of the ground states of three archaeal rhodopsins: BR[33] (PDB-entry 1qhj; 1.9 Å resolution), HR[37] (PDB-entry 1e12; 1.8 Å resolution), and SRII[38] (PDB-entry 1jgj; 2.4 Å resolution). For all structures, hydrogen atoms were generated using the HBUILD routine of CHARMM[54] and their positions were optimized by 5,000 steps of steepest descent and 5,000 steps of conjugate gradient minimization. All non-hydrogen atom coordinates were constraint during the minimization. The chloride ion found in HR below the retinal Schiff base is included in all calculations. HR binds a palmitate which is located approximately parallel to helix D. This palmitate has been included in the calculations. The hydrophobic core of the membrane around the proteins was represented by a ring of uncharged dummy atoms with a radius of 1.5 Å.[55]

Continuum Electrostatic Calculations

The electrostatic potential at any position can be accessed by solving the linearized Poisson-Boltzmann equation (LPBE):

$$\nabla[\varepsilon(\mathrm{r})\nabla\phi(\mathrm{r})] = -4\pi\rho_{prot}(\mathrm{r}) + \kappa^2\phi(\mathrm{r}) \quad (1)$$

where ∇ is the gradient operator with respect to the spatial coordinates, $\varepsilon(\mathrm{r})$ is the spatially varying dielectric constant, $\phi(\mathrm{r})$ is the electrostatic potential at position r, $\rho_{prot}(\mathrm{r})$ is the charge distribution of the protein, and the square of the inverse Debye length κ^2 represents the charge distribution due to ions in the solvent.

In the present calculations, partial atomic charges were taken from the CHARMM22 parameter set.[56] The charges for the protonated retinal Schiff base were derived from a density functional calculation as described previously.[55] Atomic radii were set to 1.7 Å for carbon atoms, 1.0 Å for hydrogen atoms, 1.5 Å for oxygen atoms, 1.55 Å for nitrogen atoms, 1.8 Å for sulfur atoms, and 1.8 Å for the chloride ion. The LPBE was numerically solved using the finite difference method implemented in the MEAD suite.[57] The dielectric boundary between the protein and the solvent was derived using a probe sphere with a radius of 1.4 Å and the atomic radii as given above. The calculations were performed using dielectric constants of 80.0 for the solvent and 4.0 for the protein and the membrane environment. In all calculations, the temperature was set to 300 K and the ionic strength to 0.1 M.

The electrostatic potential along the retinal π-system was calculated in two steps. First, populations of protonation states were calculated for all three proteins. In the second step, the highest-populated protonation state was used to calculate the electrostatic potential at the retinal.

The energy of a protonation state *n*, G^n, is given by:

$$G^n = \sum_{i=1}^{N}((x_i^n - x_i^0)RT \ln 10(pH - pK_i^{intr})) + \frac{1}{2}\sum_{i=1}^{N}\sum_{j=1}^{N}(W_{ij}(x_i^n + z_i^o)(x_j^n + z_j^o)) \quad (2)$$

where N is the number of titratable sites, x_i^n determines the protonation state of site i in protonation state n, x_i^n is 0 when site i is unprotonated and 1 when it is protonated, x_i^0 is 0 or 1 depending on the reference protonation state of site i, R is the gas constant, T is the temperature, and z_i^o is the unitless formal charge of the deprotonated form of site i, −1 for acids and 0 for bases. The interaction energy W_{ij} between each pair of titratable sites and the intrinsic pK, pK_i^{intr}, the pK-shift of site i upon transfer from solution to the protein when all other titratable sites are in their uncharged form, are calculated using the LPBE. The protonation probability for each titratable residue $\langle x_i \rangle$ as a function of pH can be derived from:

$$\langle x_i \rangle = \frac{\sum_{n=1}^{2^N} x_i^n \exp(-G^n/RT)}{\sum_{n=1}^{2^N} \exp(-G^n/RT)} \quad (3)$$

where x_i^n is 1 or 0 depending on whether site i is protonated in protonation state n or not. The method to determine protonation patterns is described in detail in other publications.[57–60] The protonation states of BR, HR, and SRII were calculated at pH = 7.0. Aspartates, arginines, cysteins, glutamates, histidines, lysines, tyrosines, the retinal Schiff base, and the palmitate were considered as titratable residues. The finite-difference grids for solving the Poisson-Boltzmann equation were focused in two steps. A coarse grid with a spacing of 1 Å was used first, followed by a fine grid with a spacing of 0.25 Å. Table I lists the highest-populated protonation state at pH = 7.0 for BR, HR, and SRII. These protonation states were used to calculate the electrostatic potential along the retinal π-system.

The electrostatic potential of the proteins experienced by the retinal is calculated at the atomic centers of the retinal π-system. Accordingly, the charges of the retinal atoms were set to zero in these calculations. Three levels of focusing were used for the finite-difference lattices: first, a coarse grid with a spacing of 1 Å, followed by a finer grid with a spacing of 0.5 Å and last a grid with a spacing of 0.25 Å.

RESULTS AND DISCUSSION

In the present article, we calculate the classical electrostatic potentials of BR, HR, and SRII at the retinal. For

TABLE I. Highest-Populated Protonation States of BR, HR, and SRII at pH = 7.0

BR		HR		SRII		BR		HR		SRII	
		R24	1					C145	1		
		E25	0			K129	1				
R7	1									E122	0
E9	0					R134	1	R161	1	R123	1
K30	1							C169	1		
		R52	1	R27	1			D182	0		
				D28	0					E147	0
		R55	1			K159	1				
D36	0					E161	0				
D38	0	R58	1	E33	0					R152	1
K40	1	R60	1	R34	1	R164	1				
K41	1			R35	1	E166	0				
		E90	0							K157	1
		H95	0					E194	0		
E74	0	E100	0	E65	0	K172	1	D197	0		
				R66	1					R162	1
		R103	1			R175	1	R200	1	R164	1
R82	1	R108	1	R72	1	E194	0	E219	0		
D85	0			D75	0	E204	1			D193	0
D96	1					D212	0	D238	0	D201	0
D102	0	D128	0			R225	1	R251	1	D214	0
D104	0	D130	0	D94	0	R227	1				
				R96	1			E257	0		
				E97	0			R258	1		
D115	1	D141	1			E232	0				

In the table, 0 indicates that the residue is deprotonated, 1 that the residue is protonated. Corresponding residues are aligned. The retinal Schiff base was found to be protonated in all three proteins. The palmitate of HR was found to be protonated. The protonation states given above were used to calculate the electrostatic potential at the retinal.

this calculation, the retinal charges are set to zero, allowing for a comparison between the different protein environments to which the retinal is exposed. The aim of this work is to identify structural differences among the archaeal rhodopsins that contribute to their different absorption behaviors. We term the absorption shift between the archaeal rhodopsins *inter-protein shift*, which is defined as the magnitude of the absorption shift between the archaeal rhodopsins. The inter-protein shift may in principle originate from differences in either steric or electrostatic interaction between the protein and the chromophore. However, experimental data[33,34,38,39,47–50] and theoretical studies[9,10] demonstrate that differences in chromophore geometry are negligible for the inter-protein shift. Thus, the environment of retinal, specifically the electrostatic interaction of the protein with the retinal, has a dominant role for the inter-protein shift.

A prerequisite for the calculation of the electrostatic potential of a protein is the determination of its protonation state. We determined the highest-populated protonation state at pH = 7.0 by electrostatic calculations for BR, HR, and SRII. The results are in excellent agreement with experimental data[37,61–63] and previous calculations of protonation states.[64,65] The retinal Schiff base was found to be protonated in all three proteins. Asp115 in BR is protonated and also the corresponding Asp141 in HR which is in agreement with its location in a highly apolar region. Apart from Asp115, two other titratable sites are not in their reference state at pH = 7.0: Asp96 and Glu204 were found to be protonated. Glu204 and another glutamate, Glu194, which are in close proximity and face each other, are both part of the proton release complex. The exact nature of this complex has been discussed for a long time. In the ground state of BR, one proton is bound to the proton release complex that is released to the extracellular site during the photocycle. The exact location of this proton, however, is still under debate. Spectroscopic measurements[66,67] as well as calculations[64] indicate that this proton is localized within a network of internal water molecules which are stabilized by Glu194 and Glu204. However, because the distance between proton release complex and retinal is large, the exact location of the proton within the proton release complex has little influence on the electrostatic potential at the retinal Schiff base. In HR, the protonation of all titratable residues, with the exception of Asp141, corresponds to the reference protonation form at pH = 7.0. For SRII, all titratable residues were found to be in their reference protonation form at pH = 7.0.

Protein Electrostatic Potential at the Retinal

Figure 3 shows the electrostatic potential of BR, HR, and SRII at the van der Waals surface of the retinal. The general features of the potential are similar for all three proteins: the potential is close to neutral in the β-ionone ring region and negative in the Schiff base region. The difference between the potential in the β-ionone ring region and the potential in the Schiff base region is,

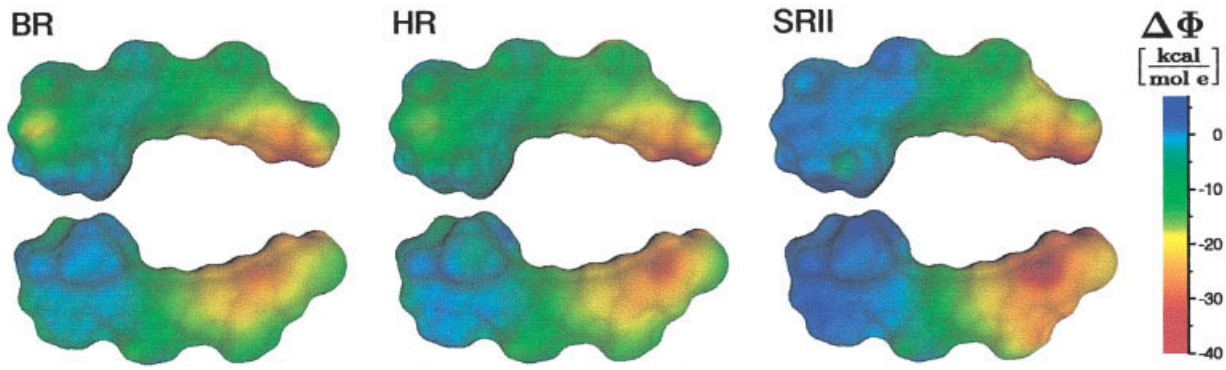

Fig. 3. Electrostatic potential of BR, HR, and SRII at the van der Waals surface of the retinal. The magnitude of the potential is color coded.

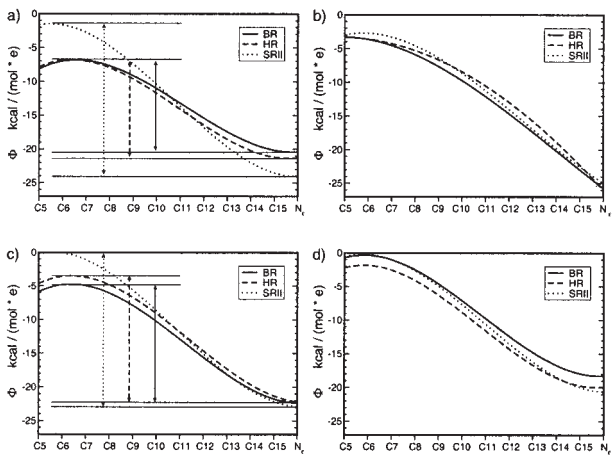

Fig. 4. Electrostatic potential along the π-system of retinal for BR, HR, and SRII: (**a**) electrostatic potential of the whole protein; (**b**) electrostatic potential of the counterion; (**c**) electrostatic potential of the binding pocket for BR, HR, and SRII plus the potential of Arg82, Arg108, and Arg72, respectively. These were included to allow a quantitative comparison between graphs a–d. In (**b**) it is shown that this arginine does not contribute to the difference among BR, HR, and SRII. In (**d**) the electrostatic potential of the protein is shown omitting the residues that were found to cause the difference among the electrostatic potential at the retinal. Arrows indicate the magnitude of the difference in potential between Schiff base and β-ionone ring. A polynomial regression was used to display the potentials.

however, more pronounced in SRII than in BR and HR. Thus, this representation indicates a greater similarity for BR and HR compared with SRII, which is in agreement with the small inter-protein shift between BR and HR compared with the large inter-protein shift between BR and SRII.

To quantify the difference between the electrostatic potentials of the three archaeal rhodopsins, the electrostatic potentials were calculated at the atomic centers of the π-system of retinal. The resulting potentials are shown in Figure 4(a). Two aspects of the electrostatic potential will be discussed in this article: i) the variation of the potential along the retinal π-system in one protein, and ii) the dissimilarity between the potentials of the archaeal rhodopsins. In all three proteins, the electrostatic potential changes from close to neutral at the β-ionone ring to negative at the Schiff base. The main dissimilarity between the archaeal rhodopsins is the magnitude of the potential difference between the β-ionone ring and the Schiff base. This difference is about 10 kcal mol^{-1} e^{-1} greater in SRII than in BR and HR, as indicated in Figure 4(a).

How is this variation of the electrostatic potential along the retinal π-system related to the observed inter-protein shift? It is known from experiments that the dipole moment of a protonated retinal Schiff base changes upon excitation. The π-electrons move toward the Schiff base and, thus, the positive charge of the Schiff base delocalizes over the retinal.[68] Interactions that stabilize the excited state, i.e., the charge delocalized state, lower the excitation energy and therefore shift the absorption maximum to the red. In contrast, interactions that stabilize the charge on the Schiff base lead to a blue shift of the absorption maximum. Because of the more pronounced difference between the electrostatic potential at the β-ionone ring and the electrostatic potential at the Schiff base in SRII, the positive charge on the Schiff base is more stabilized in SRII compared with BR and HR. Thus, in SRII, the transition energy between the ground state and the first excited state should be increased compared with BR and HR. This implication is consistent with the measured absorption spectra of the three archaeal rhodopsins shown in Figure 1(b).

Decomposition of the Electrostatic Potential

To understand the structural basis of the differences between BR, HR, and SRII, the electrostatic potential was decomposed into individual components. In particular, we analyzed the influence of the Schiff base counterion and the residues of the near retinal environment (the retinal binding pocket). Furthermore, we searched for all residues that contribute significantly to the difference in electrostatic potential between the archaeal rhodopsins.

The counterion complex

The counterion complexes of BR, HR, and SRII are depicted in Figure 5. In all three proteins, the counterion of the positively charged Schiff base consists of an arrangement of one positive and two negative charges. The positive charge originates from an arginine in all three

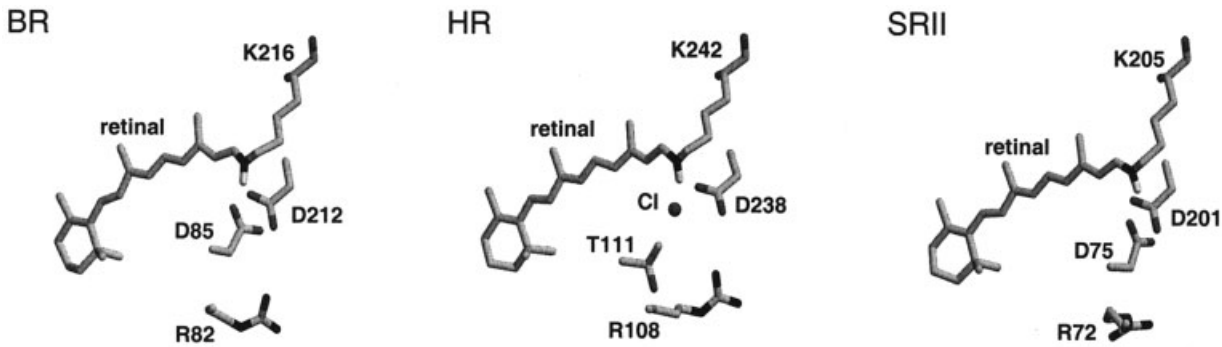

Fig. 5. The counterion of BR, HR, and SRII. Two negative charges are located beneath the retinal Schiff base, these are in the case of BR and SRII two aspartates (Asp85 and Asp212; and Asp75 and Asp201, respectively) and in the case of HR one aspartate (Asp238) and one chloride ion. A positively charged arginine is located beneath the negative charges in all three proteins (Arg82 in BR, Arg108 in HR, and Arg72 in SRII).

proteins. The negative charges originate either from two aspartates in BR and SRII, or from an aspartate and a chloride ion in HR. The chloride ion in HR takes the position of the missing aspartate carboxyl group. The aspartate itself is substituted by a threonine.

It is known from model compounds that changes in the distance between the Schiff base and the counterion complex influence the absorption maximum.[19,69–71] A shorter distance, i.e, a stronger interaction, causes a blue-shift of the absorption spectrum. However, an analysis of the X-ray structures of the archaeal rhodopsins does not reveal significant differences between the proteins. The distances between the counterion atoms and the Schiff base are given in Table II. The main difference between SRII and BR is the orientation of the arginine side-chain (Fig. 5). In a QM/MM calculation, it was found that upon structure optimization Asp201 of SRII moves toward the retinal Schiff base.[9] As shown in Hayashi et al.,[9] such a displacement would imply that Asp201 dominates the inter-protein shift between SRII and BR. Similar calculations by Ren et al.[10] showed that without this displacement Asp201 loses its dominant role. In contrast to Hayashi et al.,[9] Ren et al.[10] suggested that the orientation of Arg72 is the main cause for the inter-protein shift between SRII and BR.

To quantify the interaction between the counterion complex and the retinal, the electrostatic potential of the counterion at the retinal was calculated for BR, HR, and SRII. All backbone and side-chain atoms of the counterion residues as well as the chloride ion were included in these calculations. Figure 4(b) shows that the electrostatic potential due to the counterion is very similar in all three proteins. A comparison between Figure 4(a and b) reveals that the main contribution to the total electrostatic potential at the retinal originates from the counterion residues. This observation is not surprising, because the only charged residues close to the retinal are the counterion residues. However, the counterion complex is not the origin of the observed dissimilarity between the electrostatic potentials of BR and HR on the one hand, and SRII on the other hand. A comparison of the potentials of each individual counterion residue leads to the same conclusion. However, it should be kept in mind that the calculations presented here are based on the ground state (S_0) charge distribution. A possible influence of the counterion on the inter-protein shift may originate from polarization effects in the first excited state (S_1). Nevertheless, the dominant role of a single counterion residue found in QM/MM calculations[9,10] cannot be confirmed by our calculations of the electrostatic potential resting on the known crystal structures.

The retinal binding pocket

In the next step, we analyzed the influence of the residues in the near retinal environment on the retinal. Residues located within 5.0 Å of the heavy atom centers of the retinal Schiff base [atoms C1 to C20 and the Schiff base nitrogen; see Fig. 1(a)] are considered to form the retinal binding pocket [see highlighted residues in the sequence alignment of Fig. 2(b)]. This definition of the retinal binding pocket closely resembles those given in previous publications.[9,10,21]

The residues of the binding pocket are highly conserved among the archaeal rhodopsins [Fig. 2(b)]. Three differences between SRII and the other two proteins, BR and HR, are, however, notable: 1) Thr204 of SRII which is located close to the Schiff base is an alanine in BR (Ala215) and in HR (Ala241); 2) Gly130 of SRII which is located close to the β-ionone ring is a serine in BR (Ser141) and in HR (Ser168); and 3) Ala131 of SRII which is also located close to the β-ionone ring is a threonine in BR (Thr142) and a cysteine in HR (Cys169). Thus, in SRII, the β-ionone ring region is more apolar and the Schiff base region more polar than in BR and HR. The increased polarity of the ring region found for BR and HR might facilitate charge dislocation upon excitation, thus lowering the excitation energy compared with SRII.[9,53]

The electrostatic potential caused by the residues of the binding pocket is shown in Figure 4(c). The potential of Arg82, Arg108, and Arg72 is added to the potential of the binding pocket residues of BR, HR, and SRII, respectively, although this arginine is located more than 8 Å away from the retinal (see Table II) and is thus not part of the binding pocket. However, because this arginine contributes largely

TABLE II. Distances Between the Retinal Schiff Base Nitrogen Atom and Selected Atoms of the Counterion Residues of BR, HR, and SRII†

	Asp85[a]			Asp212[a]			Arg82[a]			
	$O_{\delta 1}$	$O_{\delta 2}$	Average	$O_{\delta 1}$	$O_{\delta 2}$	Average	N_{ε}	$N_{\eta 1}$	$N_{\eta 2}$	Average
BR	3.7	4.2	4.0	4.0	5.2	4.6	10.8	8.5	10.7	10.0
HR	3.8[b]		3.8	3.5	4.3	3.9	9.1	7.2	9.4	8.6
SRII	4.2	4.0	4.1	3.8	4.9	4.4	9.3	10.9	11.2	10.5

†All distances are given in Angstrom.
[a]The residue numbers correspond to BR. Asp85 is Thr111 and a chloride ion in HR and Asp75 in SRII. Asp212 is Asp238 in HR and Asp201 in SRII. Arg82 is Arg108 in HR and Arg72 in SRII.
[b]Distance between the chloride ion and the Schiff base nitrogen atom.

to the potential at the retinal but not to the differences among BR, HR, and SRII (see section above), it is included to allow a quantitative comparison between the graphs shown in Figure 4. The difference between the electrostatic potential at the β-ionone ring and the Schiff base is about 5 kcal mol^{-1} e^{-1} greater in SRII than in BR and HR. If the full protein is considered, this difference is about 10 kcal mol^{-1} e^{-1} greater in SRII than in BR and HR. Thus, the retinal binding pocket contributes about 50% to the dissimilarity in electrostatic potential between the archaeal rhodopsins. Shimono et al.[21] showed that the mutation of the retinal binding pocket in SRII to the wild type binding pocket of BR leads to a 25-nm red-shift of the absorption maximum, thus accounting for about 35% of the total inter-protein shift between BR and SRII. In agreement with these experiments, our result suggests that the residues of the binding pocket do have an important role for the differences between BR, HR, and SRII. Furthermore, the experiments and our calculation indicate that residues outside the binding pocket significantly contribute to the different absorption behaviors of BR, HR, and SRII.

The contribution of every binding pocket residue to the electrostatic potential was investigated and compared for the three archaeal rhodopsins, to identify those residues that are responsible for the differences in electrostatic potential. Two residues were found to contribute significantly to the dissimilarity among the potentials of BR, HR, and SRII. These two residues are Ser141 in BR (corresponding to Ser168 in HR and Gly130 in SRII) and Ala215 in BR (corresponding to Ala241 in HR and Thr204 in SRII). A smaller contribution was found for Thr142 in BR, which corresponds to Cys169 in HR and Ala131 in SRII. All three residues were discussed above to produce a different polarity in the binding pockets of BR, HR, and SRII. Thr204 in SRII generates a negative potential close to the Schiff base, whereas Ala215 in BR and Ala241 in HR generate a slightly positive potential close to the Schiff base [Fig. 6(a)]. A minor contribution of Thr204 to the inter-protein shift has also been found in QM/MM studies.[9,10] Gly130 in SRII does not contribute significantly to the potential along the retinal π-system, whereas Ser141 in BR and Ser168 in HR generate a negative potential close to the β-ionone ring [Fig. 6(b)]. Ala131 in SRII and Cys169 in HR do not contribute significantly to the potential along the retinal π-system, whereas Thr142 in BR

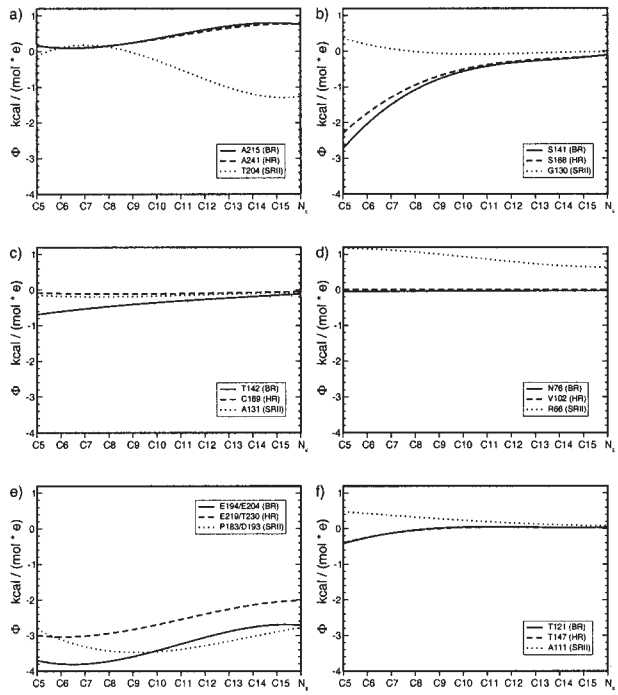

Fig. 6. Electrostatic potential of the residues that contribute to the dissimilarity between BR, HR, and SRII along the π-system of retinal. The potentials of residues from BR, HR, and SRII are shown with a solid, dashed, and dotted line, respectively: (**a**) potential of Ala215, Ala241, and Thr204; (**b**) potential of Ser141, Ser168, and Gly130; (**c**) potential of Thr142, Cys169, and Ala131; (**d**) potential of Asn76, Val102, and Arg66; (**e**) sum of the potentials of Glu194 and Glu204, Glu219 and Thr230, and Pro183 and Asp193; (**f**) potential of Thr121, T147, and Ala111. A polynomial regression was used to display the potentials.

generates a negative potential close to the β-ionone ring [Fig. 6(c)]. For the corresponding residues Thr142 (BR), Cys169 (HR), and Ala131 (SRII), a different potential is observed for BR and SRII whereas the potential of HR is similar to the potential of SRII and not BR. However, the contribution to the difference between the proteins is small compared to Ser141 (BR) and Ala215 (BR) and the corresponding residues in HR and SRII. The order of the discussed residues by magnitude of contribution to the dissimilarities among BR, HR, and SRII is: 1. Ala215 (BR), Ala241 (HR), and Thr204 (SRII); 2. Ser141 (BR), Ser168 (HR), and Gly130 (SRII); and 3. Thr142 (BR), Cys169 (HR), and Ala131 (SRII) [Fig. 6(a)]. None of the other binding pocket residues did reveal significant differences

among the proteins. Shimono et al.[21,53] measured the absorption of several mutants of SRII, where single or multiple binding pocket residues of SRII are mutated to the corresponding residues of BR. The order of the SRII single mutants by magnitude of observed red-shift is: 1. Thr204Ala, 2. Gly130Thr, and 3. Ala131Thr.[21] Thus, the differences we observe among BR, HR, and SRII and the order by magnitude of contribution is in excellent agreement with the mutational studies. Shimono et al.[21] found two other mutations that red-shift the spectrum of SRII by as much as the Ala131Thr mutant: Ile43Val and Val108Met. For these residues, we could not observe a significant difference in electrostatic potential among BR, HR, and SRII. However, because isoleucin and methionine have large side-chains, whereas valine does not, it cannot be excluded that these mutations significantly affect the structure of SRII. Shimono et al.[53] generated the double mutant G130S/T204A of SRII. The absorption maximum of the resulting SRII mutant is 512 nm, thus about 20% of the inter-protein shift is observed.[53] Our result strengthens the finding that Gly130 and Thr204 of SRII have an important role in the inter-protein shift, whereas Ala131 in SRII seems less important. Other binding pocket residues did not show significantly different contributions to the electrostatic potential at the retinal for the three proteins.

Identifying contributions from residues outside the binding pocket

To find all residues that contribute significantly to the dissimilarity among the electrostatic potentials of the proteins, we determined the contribution of each residue individually. The structures of BR, HR, and SRII were superimposed to align corresponding residues [Fig. 2(b)]. The loop regions of the archaeal rhodopsins differ in structure and number of residues and, thus, not all loop residues could be aligned. The contribution of these residues to the electrostatic potential at the retinal is, however, negligible.

The electrostatic potential at the retinal was decomposed into the contribution of individual residues. The potentials of corresponding residues were then compared for BR, HR, and SRII. First, those residues were identified for which the potentials differ by more than 1.0 kcal mol^{-1} e^{-1} anywhere along the π-system of retinal. A group of eleven such residues was found. Ser141 in BR (corresponding to Ser168 in HR and Gly130 in SRII) and also Ala215 in BR (corresponding to Ala241 in HR and Thr204 in SRII), discussed in the section above, belong to this group [see Fig. 6(a and b)]. Three more residues that contribute to the dissimilarity among the archaeal rhodopsins could be identified. These residues are Asn76 in BR (corresponding to Val102 in HR and Arg66 in SRII) and Glu194 and Glu204 in BR (corresponding to Glu219 and Thr230 in HR and to Pro183 and Asp193 in SRII). These three residues are more than 8 Å away from the retinal [Fig. 2(a)]. The electrostatic potential of Arg66 in SRII is positive along the π-system of retinal with a maximum close to the β-ionone ring, whereas the potential of the corresponding residues in BR and HR (Asn76 and Val102, respectively) is neutral along the retinal π-system [Fig. 6(d)]. Glu194 and Glu204 in BR which are in close proximity and face each other are part of the proton release complex. We find that the proton resides on Glu204 (Table I). Thus, Glu204 is neutral and Glu194 in BR is negatively charged. Glu219 in HR, corresponding to Glu194 in BR is also charged, whereas SRII has a proline (Pro183) at this position. However, Asp193 in SRII is negatively charged, whereas the corresponding Glu204 in BR is protonated, and Thr230 in HR is uncharged. Because all three proteins carry one negative charge in the region of the proton release complex of BR, we regard these two residues as one group. Thus, we compared the sum of the potentials of Glu194 and Glu204 in BR to the sum of the potentials of Glu219 and Thr230 in HR and to the sum of the potentials of Pro183 and Asp193 in SRII [Fig. 6(e)]. The potential caused by these two residues is more positive along the whole retinal π-system in HR compared with BR, whereas the potential in SRII is similar to the potential in BR in the Schiff base region, and significantly more positive at the β-ionone ring. None of the other residues in this group of 11 residues revealed significant differences among the three proteins.

Next, residues that differ by more than 0.5 kcal mol^{-1} e^{-1} anywhere along the retinal π-system were identified. Twenty-six such residues were found, among them the eleven residues that differ by more than 1.0 kcal mol^{-1} e^{-1}. The analysis of the individual contributions of these residues revealed one additional residue that contributes significantly to the dissimilarity between the electrostatic potentials of the archaeal rhodopsins. The electrostatic potential of Ala111 in SRII is nearly 1.0 kcal mol^{-1} e^{-1} more positive close to the β-ionone ring than the potential of the corresponding residues in BR (Thr121) and HR (Thr147) [Fig. 6(f)]. Ala111 is located close to the β-ionone ring of retinal just outside the retinal binding pocket [Fig. 2(a)].

We subtracted the potentials of the seven residues that show significant differences between BR, HR, and SRII from the total potential of the proteins [Fig. 4(d)]. As shown, nearly the whole dissimilarity between the potentials of the complete proteins is accounted for by these residues. The differences between the electrostatic potential of BR, HR, and SRII is thus a combined effect of these seven residues.

A Model for the Absorption Shift

It is far from trivial to derive the absorption spectra of a molecule from its molecular structure and to calculate consistently the effect of the environment on the spectra. Much effort has been made to understand this connection.[43–46, 72–74] For polyenes, however, the absorption maximum can be qualitatively understood from a quantum mechanical model of a particle located in a box.[75,76] In the simple model of a particle in a box, the allowed energy levels of a particle depend on the length of the box representing the extension of the polyene π-system. The excitation energy is given by the energy difference between the first two energy levels. Thus, according

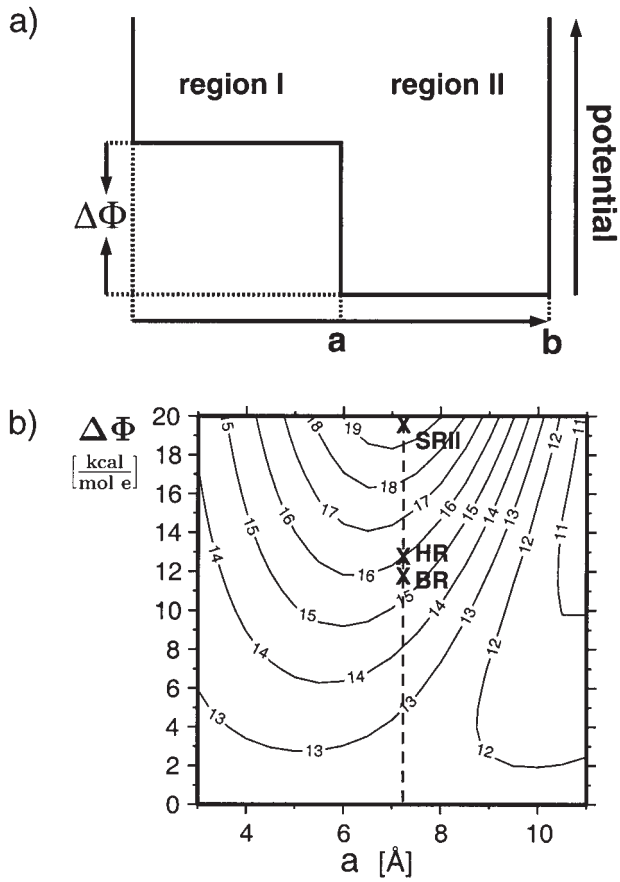

Fig. 7. (**a**) Model of a box with potential step; *b* is the length of the box, *a* the position of the step, and ΔΦ denotes the height of the potential step. (**b**) Dependence of the excitation energy Δ*E* on the position of the step *a* and the potential difference ΔΦ. The length of the box *b* is set to 14.5 Å. The excitation energy Δ*E,* given in kcal mol^{-1} e^{-1}, is indicated by the contour lines (z-direction). The dashed line marks the position of the step in the archaeal rhodopsins. The crosses indicate the height of the potential step ΔÅ for BR, HR, and SRII.

to this model, the excitation energy of a polyene depends on the extension of the π-system. In analogy, we use a variant of the model of a particle in a box to qualitatively relate differences in the electrostatic potential among the archaeal rhodopsins to changes in their absorption behavior. In comparison to the standard model of a particle in a box, the environment, here the protein, is felt by the particle as an additional potential. The electrostatic contribution of the environment is included as a step potential. A schematic picture of the resulting model is shown in Figure 7(a). The box length *b* represents the extension of the π-system. The potential step is located at position *a* and the height of the potential step is given by ΔΦ. This model provides a qualitative picture of the excitation energy of a protonated retinal Schiff base in an external electrostatic field. A detailed description of this model is given in the Appendix.

Figure 7(b) shows the excitation energy Δ*E* for a positively charged particle. The positive charge can be thought of as corresponding to the charge of the retinal Schiff base, which delocalizes over the π-system upon excitation. The box length *b* was set to 14.5 Å, representing the extension of the retinal π-system in the archaeal rhodopsins. The step position *a* and the height of the potential step ΔΦ are varied.

The qualitative picture offered by this model reveals an interesting aspect of spectral tuning. As can be seen, spectral tuning is most effective, if the controlling potential changes close to the center of the polyene π-system: then, even small changes in the height of the potential step ΔΦ have a pronounced influence on the excitation energy Δ*E*.

With these general results in mind, it is worthwhile to look again at the electrostatic potential of the three archaeal rhodopsins. Figure 4(a) reveals that two potential plateaus can be distinguished: one in the β-ionone ring region and another one in the Schiff base region. Indeed, the separation between these two plateaus is located approximately in the middle of the retinal π-system. The position of the step for the archaeal rhodopsins is indicated by the dashed line in Figure 7(b). The height of the potential step ΔΦ was defined as the difference between the potential at the β-ionone ring and the potential at the Schiff base and is indicated by the crosses for BR, HR, and SRII. The box length *b* was set to 14.5 Å, corresponding to the extension of the retinal π-system. For SRII, the excitation energy Δ*E* is significantly higher than for BR and HR, which have similar excitation energies Δ*E*. Our model thus reproduces the general trend of the measured absorption maxima by grouping BR and HR together and showing a significantly higher excitation energy for SRII (Fig. 1). This finding indicates that the observed differences in electrostatic potential in BR, HR, and SRII are related to differences in the absorption maxima.

CONCLUSIONS

In this work, we discussed the electrostatic potentials at the retinal π-system of three archaeal rhodopsins: BR, HR, and SRII. Electrostatic interactions of the retinal with the protein are likely to be the main reason for the different absorption behavior of these proteins.

The electrostatic potentials along the retinal π-system clearly differ between the archaeal rhodopsins. The potential of SRII shows a more pronounced difference between the β-ionone ring and the Schiff base than the potentials of BR and HR. The presented data show that the counterion cannot explain this difference among the electrostatic potential of BR, HR, and SRII. In agreement with mutational experiments, we could show that the retinal binding pocket contributes significantly to the difference among the electrostatic potentials at the retinal of BR, HR, and SRII. Altogether, we could identify seven residues that account for the difference among the electrostatic potential of the proteins. Three of these residues are located in the retinal binding pocket. These residues are Ser141, Thr142 and Ala215 in BR (corresponding to Ser168, Cys169 and Ala241 in HR and to Gly130, Ala131 and Thr204 in SRII). This finding is in good agreement with experimental absorption spectra of SRII single mutants. Another residue is located close to the β-ionone ring just outside the

binding pocket. This residue is Thr121 in BR, which corresponds to Thr147 and to Ala111 in HR and SRII, respectively. Three residues are located more than 8 Å away from the retinal: Asn76 in BR (corresponding to Val102 in HR and Arg66 in SRII), and Glu194 and Glu204 in BR (corresponding to Glu219 and Thr230 in HR and Pro183 and Asp193 in SRII). The electrostatic potential of the three archaeal rhodopsins at the retinal omitting these seven residues is virtually identical. The latter four residues have not been discussed before as contributing to the spectral shift among BR, HR, and SRII. However, their contribution to the difference in electrostatic potential among the archaeal rhodopsins is evident. Because three of the identified residues are located far from the retinal, future QM/MM studies on the shift among BR, HR, and SRII need to include a sufficiently large part of the protein. From our results, we conclude that the difference among the electrostatic potentials at the retinal is delocalized over seven residues that are in part close and in part far from the retinal. This delocalization may well be of evolutionary advantage, because single point mutations will not erase the differences among the proteins.

ACKNOWLEDGMENTS

The authors thank Prof. Donald Bashford for providing his program MEAD, and Prof. Jeremy C. Smith, Dr. Marcus Elstner, Dr. Ana-Nicoleta Bondar, Nicolas Calimet, Michael Hoffmann, and Marius Wanko for helpful discussions.

REFERENCES

1. Kochendoerfer GG, Lin SW, Sakmar TP, Mathies RA. How color visual pigments are tuned. Trends Biochem Sci 1999;24:300–305.
2. van der Horst MA, Hellingwerf KJ. Photoreceptor proteins, "star actors of modern times": a review of the functional dynamics in the structure of representative members of six different photoreceptor families. Acc Chem Res 2004;37:13–20.
3. Schwemer J, Langer H. Insect visual pigments. Methods Enzymol 1982;81:182–190.
4. Kleinschmidt J, Harosi FI. Anion sensitivity and spectral tuning of cone visual pigments in situ. Proc Natl Acad Sci USA 1992;89: 9181–9185.
5. Warshel A, Ottolenghi M. Kinetic and spectroscopic effects of protein-chromophore electrostatic interactions in bacteriorhodopsin. Photochem Photobiol 1979;30:291–293.
6. Houjou H, Inoue Y, Sakurai M. Physical origin of the opsin shift of bacteriorhodopsin. Comprehensive analysis based on medium effect theory of absorption spectra. J Am Chem Soc 1998;120:4459–4470.
7. Houjou H, Inoue Y, Sakurai M. Study of the opsin shift of bacteriorhodopsin: insight from QM/MM calculations with electronic polarization effects of the protein environment. J Phys Chem B 2001;2001:867–879.
8. Rajamani R, Gao J. Combined QM/MM study of the opsin shift in bacteriorhodopsin. J Comput Chem 2002;23:96–105.
9. Hayashi S, Tajkhorshid E, Pebay-Peyroula E, et al. Structural determinants of spectral tuning in retinal proteins: bacteriorhodopsin vs. sensory rhodopsin II. J Phys Chem B 2001;105:10124–10131.
10. Ren L, Martin CH, Wise KJ, et al. Molecular mechanism of spectral tuning in sensory rhodopsin II. Biochemistry 2001;40: 13906–13914.
11. Warshel A, Chu ZT. Nature of the surface crossing process in bacteriorhodopsin: computer simulations of the quantum dynamics of the primary photochemical event. J Phys Chem B 2001;105: 9857–9871.
12. Sugihara M, Buβ V, Entel P, Elstner M, Frauenheim T. 11-*cis*-Retinal protonated Schiff base: influence of the protein environment on the geometry of the rhodopsin chromophore. Biochemistry 2002;41:15259–15266.
13. Sakurai M, Sakata K, Saito S, Nakajima S, Inoue Y. Decisive role of electronic polarization of the protein environment in determining the absorption maximum of halorhodopsin. J Am Chem Soc 2003;125:3108–3112.
14. Schreiber M, Sugihara M, Buß V. Exploring the opsin shift with ab initio methods: geometry and counterion effects on the electronic spectrum of retinal. J Chem Phys 2003;119:12045–12048.
15. Wanko M, Hoffmann M, Strodel P, et al. Calculating absorption shifts for retinal proteins: computational challenges. J Phys Chem B 2005;109:3606–3615.
16. Nakanishi K, Balogh-Nair V, Arnaboldi M, Tsujimoto K, Honig B. An external point-charge model for bacteriorhodopsin to account for its purple color. J Am Chem Soc 1980;102:7945–7947.
17. Spudich JL, McCain DA, Nakanishi K, et al. Chromophore/protein interaction in bacterial sensory rhodopsin and bacteriorhodopsin. Biophys J 1986;49:479–483.
18. Takahashi T, Yan B, Mazur P, Derguini F, Nakanishi K, Spudich JL. Color regulation in the archaebacterial phototaxis receptor phoborhodopsin (sensory rhodopsin II). Biochemistry 1990;29: 8467–8474.
19. Hu J, Griffin RG, Herzfeld J. Synergy in the spectral tuning of retinal pigments: complete accounting of the opsin shift in bacteriorhodopsin. Proc Natl Acad Sci. USA 1994;91:8880–8884.
20. Lin SW, Kochendoerfer GG, Carroll KS, Wang D, Mathies RA, Sakmar TP. Mechanisms of spectral tuning in the blue cone visual pigments. J Biol Chem 1998;273:24583– 24591.
21. Shimono K, Ikeura Y, Sudo Y, Iwamoto M, Kamo N. Environment around the chromophore in *pharaonis* phoborhodopsin: mutation analysis of the retinal binding site. Biochim Biophys Acta 2001; 1515:92–100.
22. Parry JW, Poopalasundaram S, Bowmaker JK, Hunt DM. A novel amino acid substitution is responsible for spectral tuning in a rodent violet-sensitive visual pigment. Biochemistry 2004;43:8014–8020.
23. Spudich JL, Yang CS, Jung KH, Spudich EN. Retinylidene proteins: structures and functions from archaea to humans. Annu Rev Cell Dev Biol 2000;16:365–392.
24. Erickson JO, Blatz PE. N-retinylidene-1-amino-2-propanol: a Schiff base analog for rhodopsin. Vision Res 1968;8:1367–1375.
25. Tang L, Ebrey TG, Subramaniam S. Sequences and structures of retinal proteins. Isr J Chem 1995;35:193–209.
26. Haupts U, Tittor J, Bamberg E, Oesterhelt D. General concept for ion translocation by halobacterial retinal proteins: the isomerization/switch/transfer (IST) model. Biochemistry 1997;36:2–7.
27. Spudich JL. Variations on a molecular switch: transport and sensory signaling by archaeal rhodopsins. Mol Microbiol 1998;28: 1051–1058.
28. Stoeckenius W. Bacterial rhodopsins: evolution of a mechanistic model for the ion pumps. Protein Sci 1999;8:447–459.
29. Mukohata Y, Ihara K, Tamura T, Sugiyama Y. Halobacterial rhodopsins. J Biochem 1999;125:649–657.
30. Schäfer G, Engelhardt M, Müller V. Bioenergetics of the archaea. Microbiol Mol Biol Rev 1999;63:570–620.
31. Oren A. Bioenergetic aspects of halophilism. Microbiol Mol Biol Rev 1999;63:334–348.
32. Essen L-O, Siegert R, Lehmann WD, Oesterhelt D. Lipid patches in membrane protein oligomers: crystal structure of the bacteriorhodopsin-lipid complex. Proc Natl Acad Sci USA 1998;95:11673–11678.
33. Belrhali H, Nollert P, Royant A, et al. Protein, lipid and water organization in bacteriorhodopsin crystals: a molecular view of the purple membrane at 1.9 Å resolution. Structure 1999;7:909–917.
34. Luecke H, Schobert B, Richter H-T, Cartailler J-P, Lanyi JK. Structure of bacteriorhodopsin at 1.55 Å resolution. J Mol Biol 1999;291:899–911.
35. Faham S, Bowie JU. Bicelle crystallization: a new method for crystallizing membrane proteins yields a monomeric bacteriorhodopsin structure. J Mol Biol 2002;316:1–6.
36. Matsui Y, Sakai K, Murakami M, et al. Specific damage induced by X-ray radiation and structural changes in the primary photoreaction of bacteriorhodopsin. J Mol Biol 2002;324:469–481.
37. Kolbe M, Besir H, Essen L-O, Oesterhelt D. Structure of the light-driven chloride pump halorhodopsin at 1.8 Å resolution. Science 2000;288:1390–1396.

38. Luecke H, Schobert B, Lanyi JK, Spudich EN, Spudich JL. Crystal structure of sensory rhodopsin II at 2.4 angstroms: insights into color tuning and transducer interaction. Science 2001;293:1499–1502.
39. Royant A, Nollert P, Edman K, Neutze R, Landau EM, Pebay-Peyroula E. X-ray structure of sensory rhodopsin II at 2.1-Å resolution. Proc Natl Acad Sci USA 2001;98:10131–10136.
40. Goldschmidt CR, Ottolenghi M, Korenstein R. On the primary quantum yields in the bacteriorhodopsin photocycle. Biophys J 1976;16:839–843.
41. Spudich JL, Bogomolni RA. Spectroscopic discrimination of the three rhodopsinlike *Halobacterium halobium* membranes. Biophys J 1983;43:243–246.
42. Hirayama J, Imamoto Y, Shichida Y, Kamo N, Tomioka H, Yoshizawa T. Photocycle of phoborhodopsin from haloalkaliphilic bacterium (*Natronobacterium pharaonis*) studied by low-temperature spectrophotometry. Biochemistry 1992;31:2093–2098.
43. Amos AT, Burrows BL. Solvent-shift effects on electronic spectra and excited-state dipole moments and polarizabilities. Adv Quantum Chem 1973;7:289–313.
44. Warshel A. Calculation of chemical processes in solution. J Phys Chem 1979;83:1640–1652.
45. Luzhkov V, Warshel A. Microscopic calculation of solvent effects on absorption spectra of conjugated molecules. J Am Chem Soc 1991;113:4491–4499.
46. Gao J. Monte Carlo quantum mechanical-configuration interaction and molecular mechanics simulation of solvent effects on the $n \rightarrow \pi^*$ blue shift of acetone. J Am Chem Soc 1994;116:9324–9328.
47. Harbison GS, Smith SO, Pardoen JA, et al. Solid-state 13C NMR detection of a perturbed 6-s-*trans* chromophore in bacteriorhodopsin. Biochemistry 1985;24:6955–6962.
48. Baselt DR, Fodor S, van der Steen R, Lugtenburg J, Bogomolni RA, Mathies RA. Halorhodopsin and sensory rhodopsin contain a C6–C7 s-*trans* retinal chromophore. Biophys J 1989;55:193–196.
49. Sakamoto M, Wada A, Akai A, Ito M, Goshima T, Takahashi T. Evidence for the archaebacterial-type conformation about the bond between the small β-ionone ring and the polyene chain of the chromophore retinal in chlamyrhodopsin. FEBS Lett 1998;434:335–338.
50. Kandori H, Shimono K, Sudo Y, Iwamoto M, Shichida Y, Kamo N. Structural changes of *pharaonis* phoborhodopsin upon photoisomerization of the retinal chromophore: infrared spectral comparison with bacteriorhodopsin. Biochemistry 2001;40:9238–9246.
51. Warwicker J, Watson HC. Calculation of the electric potential in the active site cleft due to alpha-helix dipoles. J Mol Biol 1982;157:671–679.
52. Honig B, Nicholls A. Classical electrostatics in biology and chemistry. Science 1995;268:1144–1149.
53. Shimono K, Iwamoto M, Sumi M, Kamo N. Effects of three characteristic amino acid residues of *pharaonis* phoborhodopsin on the absorption maximum. Photochem Photobiol 2000;72:141–145.
54. Brooks BR, Bruccoleri RE, Olafson BD, States DJ, Swaminathan S, Karplus M. CHARMM: a program for macromolecular energy, minimization, and dynamics calculation. J Comput Chem 1983;4:187–217.
55. Calimet N, Ullmann GM. The influence of a transmembrane pH gradient on protonation probabilities of bacteriorhodopsin: the structural basis of the back-pressure effect. J Mol Biol 2004;339:571–589.
56. MacKerell AD, Bashford D, Bellott M, et al. All-atom empirical potential for molecular modeling and dynamics studies of proteins. J Phys Chem B 1998;102:3586–3616.
57. Bashford D. An object-oriented programming suite for electrostatic effects in biological molecules. In: Ishikawa Y, Oldehoeft RR, Reynders JVW, Tholburn M, editors. Scientific computing in object-oriented parallel environments. New York: Springer;1997. p 233–240.
58. You T, Bashford D. Conformation and hydrogen ion titration of proteins: a continuum electrostatic model with conformational flexibility. Biophys J 1995;69:1721–1733.
59. Ullmann GM, Knapp E-W. Electrostatic models for computing protonation and redox equilibria in proteins. Eur Biophys 1999;28:533–551.
60. Beroza P, Fredkin DR, Okamura MY, Feher G. Electrostatic calculation of amino acid titration and electron transfer $Q_AQ_B \rightarrow Q_AQ_{\bar{B}}$ in the reaction center. Biophys J 1995;68:2233–2250.
61. Zscherp C, Schlesinger R, Tittor J, Oesterhelt D, Heberle J. In situ determination of transient pKa changes of internal amino acids of bacteriorhodopsin by using time-resolved attenuated total reflection Fourier-transform infrared spectroscopy. Proc Natl Acad Sci USA 1999;96:5498–5503.
62. Iwamoto M, Furutani Y, Sudo Y, Shimono K, Kandori H, Kamo N. Role of Asp193 in chromophore-protein interaction of *pharaonis* phoborhodopsin (sensory rhodopsin II). Biophys J 2002;83:1130–1135.
63. Iwamoto M, Furutani Y, Kamo N, Kandori H. Proton transfer reactions in the F86D and F86E mutants of *pharaonis* phoborhodopsin (sensory rhodopsin II). Biochemistry 2003;42:2790–2796.
64. Spassov VZ, Luecke H, Gerwert K, Bashford D. pK_a calculations suggest storage of an excess proton in a hydrogen-bonded water network in bacteriorhodopsin. J Mol Biol 2001;312:203–219.
65. Song Y, Mao J, Gunner MR. Calculation of proton transfers in bacteriorhodopsin bR and M intermediates. Biochemistry 2003;42:9875–9888.
66. Rammelsberg R, Huhn G, Lubben M, Gerwert K. Bacteriorhodopsin's intramolecular proton-release pathway con-sists of a hydrogen-bonded network. Biochemistry 1998;37:5001–5009.
67. Garczarek F, Brown LS, Lanyi JK, Gerwert K. Proton binding within a membrane protein by a protonated water cluster. Proc Natl Acad Sci USA 2005;102:3633–3638.
68. Mathies R, Stryer L. Retinal has a highly dipolar vertically excited singlet state: implications for vision. Proc Natl Acad Sci USA 1976;73:2169–2173.
69. Blatz PE, Mohler JH, Navangul HV. Anion-induced wavelength regulation of absorption maxima of Schiff bases of retinal. Biochemistry 1972;11:848–855.
70. Bassov T, Sheves M. Model compounds for the study of spectroscopic properties of visual pigments and bacteriorhodopsin. J Am Chem Soc 1985;107:7524–7533.
71. Hu JG, Griffin RG, Herzfeld J. Interactions between the protonated Schiff base and its counterion in the photointermediates of bacteriorhodopsin. J Am Chem Soc 1997;119:9495–9498.
72. Banisaukas J, Szczepanski J, Eyler J, Vala M. Vibrational and electronic spectroscopy of acenaphthylene and its cation. J Phys Chem A 2003;107:782–793.
73. Halasinski TM, Weisman JL, Ruiterkamp R, Lee TJ, Salama F, Head-Gordon M. Electronic absorption spectra of neutral perrylene ($C_{20}H_{12}$), terrylene ($C_{30}H_{16}$), and quaterrylene ($C_{40}H_{20}$) and their positive and negative ions: Ne matrix-isolation spectroscopy and time-dependent density functional theory calculations. J Phys Chem A 2003;107:3660–3669.
74. Christensen RL, Barney EA, Broene RD, Galinato MGI, Frank HA. Linear polyenes: models for the spectroscopy and photophysics of carotenoids. Arch Biochem Biophys 2004;430:30–36.
75. Atkins PW, de Paula J. Atkins' physical chemistry. Oxford: Oxford University Press; 2002.
76. Tinoco I, Sauer K, Wang JC, Puglisi JD. Physical chemistry: principles and applications in biological sciences. New York: Prentice Hall; 2001.

APPENDIX

Numerical Solution for a Particle in a Box With Step Potential

The results from Figure 7b were obtained using a variant of the quantum mechanical model of a particle in a box. The standard model of a particle in a box describes the allowed energy levels of a particle in dependence on the extension of the box. For polyenes, the box extension corresponds to the length of the π-system. In our extended model of a particle in a box, the environment, here the protein, is felt by the particle as an additional potential. This additional contribution was approximated by a step potential and, thus, the allowed energy levels of a particle depend on two additional parameters, the height of the potential step and its position. A schematic picture of the resulting model is shown in Figure 7a. The box length b represents the extension of the π-system. The potential

step is located at position a and the height of the potential step is given by $\Delta\Phi$. For a particle of charge q located in this potential, the stationary Schrödinger equation is given by:

$$E\Psi(x) = -\frac{\hbar^2}{2m}\frac{\partial^2}{\partial x^2}\Psi(x) + V(x)\Psi(x) \tag{4}$$

where E is the energy of the particle, Ψ its wave function, $\hbar$ denotes Planck's constant divided by 2π, m is the mass of the particle, and V is the potential energy given by:

$$V(x) = \begin{cases} q\Phi_I & 0 < x < a \\ q\Phi_{II} & a < x < b \\ \infty & elsewhere \end{cases} \tag{5}$$

where Φ_I and Φ_{II} denote the potential of the environment in region I and region II, respectively. The boundary conditions $\Psi(0) = \Psi(b) = 0$ together with the continuity of the wave function and its derivative at $x = a$ lead to a quantization condition for the allowed energy levels:

$$\frac{1}{k_1}\frac{e^{ik_1a} - e^{-ik_1a}}{e^{ik_1a} + e^{-ik_1a}} = \frac{1}{k_2}\frac{e^{ik_2(a-b)} - e^{-ik_2(a-b)}}{e^{ik_2(a-b)} + e^{-ik_2(a-b)}} \tag{6}$$

Here, k_1 and k_2 are the wave vectors in region I and region II, respectively, given by:

$$k_i = \sqrt{2m/\hbar^2(E - q\Phi_i)} \tag{7}$$

The term $(E - q\Phi_i)$ can be negative for one of the two regions, I or II. In that case, the corresponding wave vector k_i is a complex number, $k = i\rho$, with $\rho = \sqrt{2m/\hbar^2|E - q\Phi_i|}$. The corresponding solution decays exponentially, reflecting the fact that the region is classically forbidden. Equation (6) can be solved numerically leading to a discrete energy spectrum of the system.

Two limiting cases can be distinguished: i) the step is located near the potential walls, and ii) the potential step becomes vanishingly small. When the step is close to one of the potential walls of the box, i.e., a is close to 0 or b, the model approaches the standard model of a particle in a box. Consequently, the dependence of ΔE on a and $\Delta\Phi$ is low in this limit. For the second limiting case, when the height of the potential step $\Delta\Phi$ approaches zero, a similar effect is seen and the behavior resembles again the standard model of a particle in a box.